

# Graphene-metasurface for wide-incident-angle terahertz absorption<sup>\*</sup>

Ri-hui XIONG<sup>1</sup>, Xiao-qing PENG<sup>2</sup>, Jiu-sheng LI<sup>†‡1</sup>

<sup>1</sup>Center for THz Research, China Jiliang University, Hangzhou 310018, China

<sup>2</sup>State Grid Sichuan Electric Power Company, Chengdu 610041, China

<sup>†</sup>E-mail: ljsh2008@126.com

Received Apr. 6, 2020; Revision accepted June 10, 2020; Crosschecked Aug. 18, 2020; Published online Nov. 11, 2020

**Abstract:** We demonstrate a graphene-metasurface structure for tunable wide-incident-angle terahertz wave absorption, which involves depositing planar arrays of Omega-shaped graphene patterns on a silicon dioxide substrate. We also discuss how the graphene Fermi-level layer and various substrates affect the absorption characteristics. The absorption of the proposed terahertz absorber is above 80% at an incident angle of 0°–60° in frequencies ranging from 0.82 to 2.0 THz. Our results will be very beneficial in the application of terahertz wave communications and biomedical imaging/sensing systems.

**Key words:** Graphene-metasurface; Terahertz absorber; Omega-shaped graphene patterns

<https://doi.org/10.1631/FITEE.2000079>

**CLC number:** O436.2

## 1 Introduction

Terahertz wave absorbers have attracted much attention because of the prospect of their broad application in terahertz wave detection, imaging, and biomedical sensing (Esquiús-Morote et al., 2014; He XY et al., 2019; Zhou et al., 2019). Recently, various terahertz absorbers have been proposed based on metamaterials (Hu et al., 2014; He YN et al., 2015; He XY, 2020b). However, these absorbers have a finite terahertz bandwidth and a certain terahertz frequency. Once these terahertz wave devices are designed, the dynamic tunability can be controlled only by changing the geometries. However, in many practical applications, robust tunable terahertz absorbers are very important. Recently, some tunable graphene-based terahertz devices have been presented (Othman et al., 2013; Shi et al., 2019; He XY et al.,

2020a). For example, Amin et al. (2013) demonstrated a graphene absorber based on multilayer graphene. Zhang Y et al. (2014) realized a polarization-independent absorber using graphene with embedded cross-shaped metallic resonators. Su et al. (2015) proposed a terahertz absorber using multilayer graphene/MgO<sub>2</sub>. Long et al. (2018) demonstrated a terahertz absorber based on a graphene-metasurface hybrid structure. Liu Y et al. (2019) designed a terahertz wave absorber using multilayer graphene metamaterial. In recent years, many graphene-patterned terahertz devices have been reported (Xiao et al., 2016, 2019; Liu TT et al., 2019a, 2019b), but these works usually consider only ideal cases in simulation and cannot provide experimental results that verify the simulation. Under current fabrication conditions, however, it is very difficult to produce the patterned-graphene structure. Despite the demonstration of various terahertz absorbers, a high-efficiency, polarization-insensitive, wide-incident-angle terahertz wave absorber is still needed.

Our goal is to explore a new tunable broadband terahertz wave absorber with a very wide incident

<sup>‡</sup> Corresponding author

<sup>\*</sup> Project supported by the Zhejiang Lab (No. 2019LC0AB03)

© Zhejiang University and Springer-Verlag GmbH Germany, part of Springer Nature 2020

angle range, which is also compact and not sensitive to polarization. We propose a novel tunable broadband terahertz absorber that involves depositing Omega-shaped graphene patterns on a silicon dioxide substrate. We analyze the absorption mechanism and characteristics of the terahertz absorber by changing the graphene Fermi level, pattern size, substrate thickness, and terahertz wave incident angle. The proposed absorber achieves absorption above 80% at an incident angle interval from  $0^\circ$  to  $60^\circ$  in the frequency range of 0.82–2.0 THz. This wide incident angle range and tunable terahertz wave absorber approach can be widely used in terahertz wave detection, communications, imaging, security, and biomedical sensing.

## 2 Device structure

Fig. 1 depicts the geometry and sizes of the proposed graphene-metasurface terahertz absorber structure. Planar arrays of Omega-shaped-graphene patterns are deposited on a silicon dioxide substrate, in which the unit cell consists of an Omega-shaped graphene metasurface structure and a copper mirror, separated by a silicon-dioxide layer. The relative permittivity ( $\epsilon_r$ ) and silicon-dioxide thickness are 3.9 and  $30 \mu\text{m}$ , respectively. The bottom copper ground plane layer conductivity ( $\sigma$ ) and thickness are  $5.8 \times 10^7 \text{ S/m}$  and  $0.5 \mu\text{m}$ , respectively. The two bias electrodes are located at the top and bottom of an ionic gel layer. The refractive index of ionic gel is 2 in the terahertz range. In our proposed structure, the graphene thickness is  $0.5 \text{ nm}$  and the meshing density is  $0.15 \text{ nm} \times 0.15 \text{ nm} \times 0.15 \text{ nm}$ . The proposed terahertz wave absorber has been studied and simulated using the commercial finite element method software CST Microwave Studio simulator. The terahertz wave is perpendicularly incident to the proposed terahertz wave absorber along the  $z$  axis. Fig. 1b shows the top view of the unit cell. The following are the parameters of the optimized terahertz wave absorber:  $P=50 \mu\text{m}$ ,  $R=12 \mu\text{m}$ ,  $r=4 \mu\text{m}$ ,  $w=5 \mu\text{m}$ , and  $s=13 \mu\text{m}$ . This optimization creates the absorption curves of the Omega-shaped graphene-metasurface structure and its complementary structure as shown in Fig. 1c. In Fig. 1c, note that the non-complementary symmetrical graphene structure can attain an absorption of

only 77% at 1.32 THz with a narrow absorption bandwidth. To ensure a proper absorption bandwidth, a complementary symmetrical Omega-shaped graphene pattern has been designed as a terahertz broadband absorber. The Omega-shaped graphene patterns can be fabricated by large-scale synthesis, transfer, and etching technique, and electron beam lithography can be employed to produce Omega patterns on the graphene layer (Kim et al., 2009; Jo et al., 2010). The chemical vapor deposition method is one of the best methods for fabricating this type of multi-layer structure.

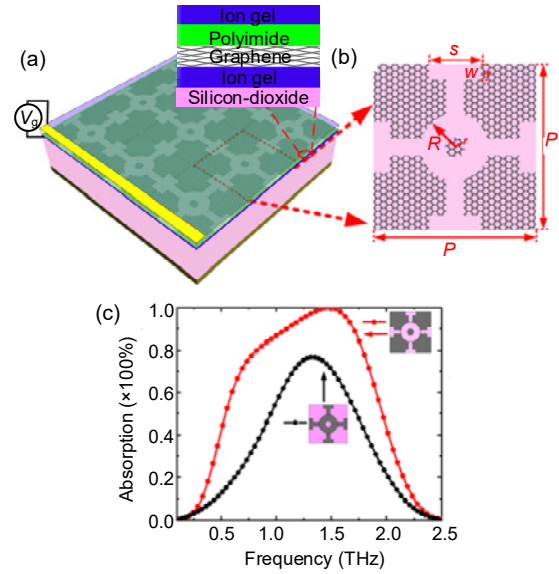


**Fig. 1** Three-dimensional schematic of the terahertz absorber (a), Omega-shaped graphene metasurface structure unit cell (b), and terahertz wave absorption curves of Omega-shaped graphene metasurface structure and its complementary structure (c)

The graphene conductivity has both intraband and interband contributions by transition and in-band electron-photon scattering, which can be described by the Kubo relation (Zhang YB et al., 2005):

$$\sigma = \sigma_{\text{intra}} + \sigma_{\text{inter}} = \frac{2e^2 k_B T}{\pi h^2} \frac{i}{\omega + i\tau^{-1}} \ln \left[ 2 \cosh \left( \frac{E_F}{2k_B T} \right) \right] + \frac{e^2}{4h} \left[ \frac{1}{2} + \frac{1}{\pi} \arctan \left( \frac{h\omega - 2E_F}{2k_B T} \right) \right] - \frac{e^2}{4h} \left[ \frac{i}{2\pi} \ln \frac{(h\omega + 2E_F)^2}{(h\omega - 2E_F)^2 + 4(k_B T)^2} \right], \quad (1)$$

where  $e$  represents the electron charge,  $k_B$  the Boltzmann constant,  $T$  the Kelvin temperature,  $h$  Planck's constant,  $i$  the imaginary unit,  $\omega$  the angular frequency,  $\tau$  the carrier relaxation time, and  $E_F$  the graphene's Fermi energy. For the heavily doped graphene at the terahertz frequency considered here, i.e.,  $E_F \gg h\omega \gg k_B T$ , the intraband contribution is dominant and the graphene's conductivity,  $\sigma$ , can be described by a Drude-like model expression as follows (Jnawali et al., 2013; Zhang JF et al., 2016):

$$\sigma = \frac{e^2 E_F}{\pi h^2} \frac{i}{\omega + i\tau^{-1}}, \quad (2)$$

where the carrier relaxation time is  $\tau = \mu E_F / (ev_F^2)$ , the carrier mobility is  $\mu = 10\,000 \text{ cm}^2/(\text{V}\cdot\text{s})$ , and the Fermi velocity is  $v_F \approx 1.1 \times 10^6 \text{ m/s}$ . The graphene's conductivity can be adjusted by changing the Fermi level (i.e., chemical potential,  $\mu_c$ ) with biasing voltage.

### 3 Results and discussion

We performed calculations by CST software to study the absorption of the proposed terahertz wave absorber. The periodic boundary conditions were used in the  $x$ - $y$  plane. Fig. 2a shows the absorption spectra with different chemical potentials  $\mu_c$  of the proposed absorber. We varied  $\mu_c$  using the interval from 0.4 to 0.6 eV with a pitch of 0.1 eV. From the figure, it can be noted that the terahertz wave absorption in the 1.36–1.54 THz frequency bandwidth range was close to perfect absorption (above 99.5%) when  $\mu_c = 0.5 \text{ eV}$ . The absorption also exceeded 90% in the 1.05–1.69 THz frequency range. In this paper, relative absorption bandwidth is defined as  $\text{BW} = 2(f_{\text{max}} - f_{\text{min}}) / (f_{\text{max}} + f_{\text{min}})$ , where  $f_{\text{max}}$  is the maximum frequency at which the absorption spectrum of the designed terahertz wave absorber is above 90%, and  $f_{\text{min}}$  is the minimum frequency at which the absorption spectrum of the designed terahertz wave absorber is above 90%. The relative bandwidth of the designed graphene-metasurface terahertz wave absorber was about 37% when  $\mu_c = 0.5 \text{ eV}$ . In the 0.8–1.78 THz frequency range, the absorption was more than 80%. When  $\mu_c = 0.4 \text{ eV}$ , the absorption

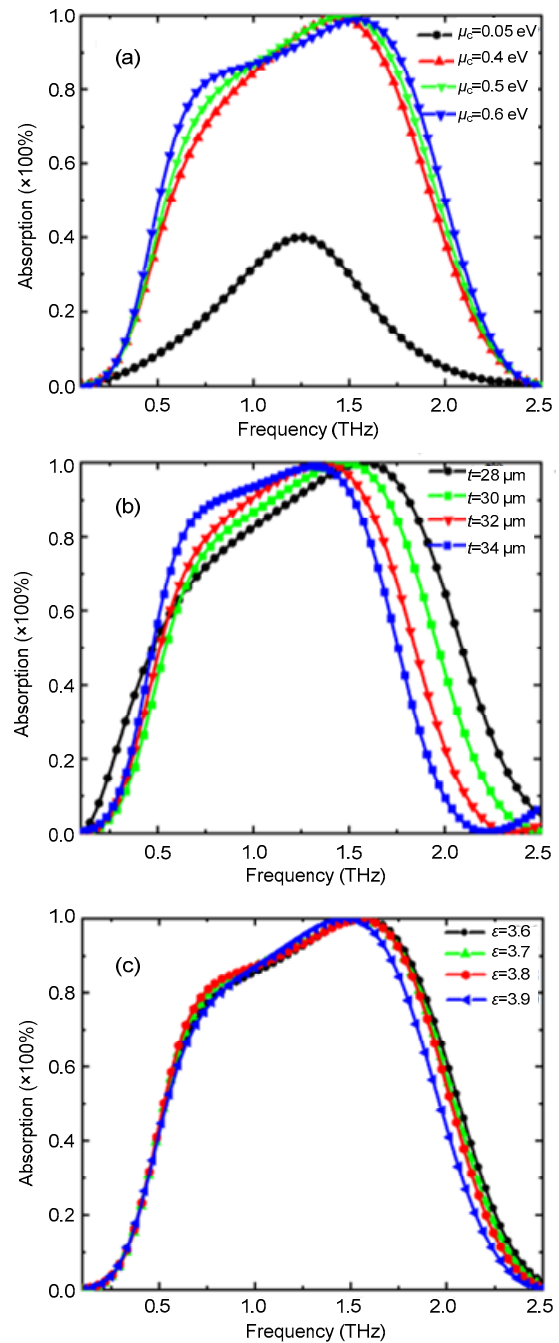


**Fig. 2** Absorption spectra for various chemical potentials  $\mu_c$  (a), substrate thicknesses  $t$  (b), and dielectric constants  $\varepsilon$  (c)

bandwidth became narrow. The frequency ranges of the absorber were 1.12–1.62 and 0.93–1.71 THz when the absorption exceeded 90% and 80%, respectively. Note that a larger  $\mu_c$  led to a wider absorption bandwidth. As  $\mu_c$  increased to 0.6 eV, the absorption was close to perfect absorption in the

1.48–1.58 THz frequency range. In the 1.11–1.75 THz frequency range, the absorption was more than 90% and the relative bandwidth was about 35%. In addition, in the 0.71–1.83 THz frequency range, the absorption exceeded 80%. When  $\mu_c=0.05$  eV, the maximum absorption was only 36%.

We also investigated the influence of inter-layer thickness ( $t$ ), from 28 to 34  $\mu\text{m}$  with a pitch of 2  $\mu\text{m}$  (Fig. 2b). We found that the absorption above 90% occurred in the 1.24–1.83, 1.05–1.69, 0.97–1.59, and 0.9–1.50 THz frequency ranges, and the corresponding relative bandwidths were 29%, 37%, 38%, and 40%, respectively. Also, note that the resonance frequency moved to the low-frequency range when the inter-layer thickness increased. Fig. 2c shows the relationship between the different dielectric constants and the absorption spectrum. When the dielectric constant of the inter-layer changed from 3.6 to 3.9, the bandwidths of the proposed absorbers with absorption above 90% were 1.15–1.80, 1.12–1.76, 1.11–1.72, and 1.05–1.69 THz, and the corresponding relative bandwidths were 34.5%, 35%, 34.3%, and 37%, respectively. The absorption frequency showed a slight red shift due to the increase of the dielectric constant of the intermediate dielectric layer. Fig. 3 shows the absorption spectrum of TE- and TM-polarized mode under normal incidence when  $\mu_c=0.5$  eV. Note that the terahertz absorption bandwidth of the proposed absorber with absorption above 90% was from 1.07 to 1.69 THz when the incident terahertz wave was TE-polarized. The absorption spectrum of TM polarization showed a trend similar to that of TE polarization.

Fig. 4 shows the electric field distribution of the Omega-shaped graphene-metasurface terahertz wave absorber. Figs. 4a and 4b depict the electric field distributions of the proposed terahertz absorber at a non-resonance frequency ( $f=0.4$  THz) and the resonance frequency ( $f=1.5$  THz), respectively. For the TE-polarized wave, a strong electric field was concentrated at left and right symmetry of the central ring along the  $y$  axis, and the electric field binding at  $f=1.5$  THz was significantly stronger than that at  $f=0.4$  THz. Thus, the absorption at the resonance frequency was enhanced significantly. For the TM polarization wave, Figs. 4c and 4d depict the electric field distribution at non-resonance frequency  $f=0.4$  THz and resonance frequency  $f=1.5$  THz, respectively. A strong electric field was distributed in the upper and

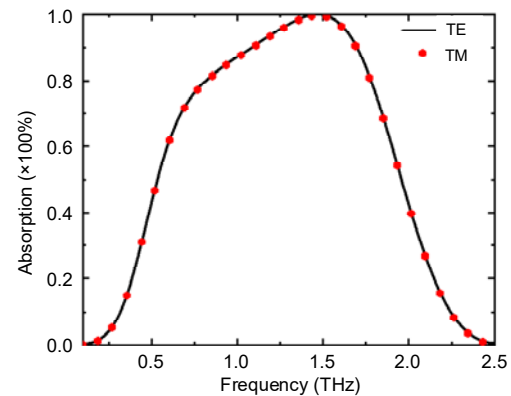


Fig. 3 Absorption of TE- and TM-polarized modes

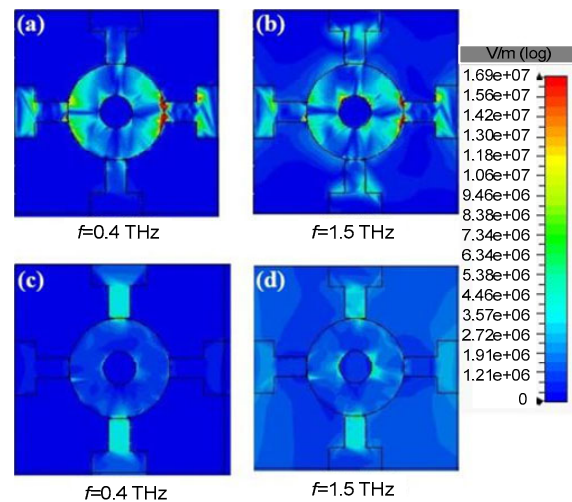
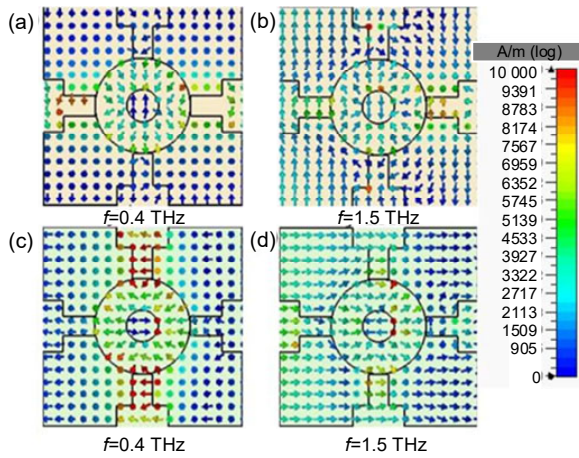


Fig. 4 Electric field distributions: (a) TE polarization at  $f=0.4$  THz; (b) TE polarization at  $f=1.5$  THz; (c) TM polarization at  $f=0.4$  THz; (d) TM polarization at  $f=1.5$  THz

lower symmetrical T-shaped structure. The surface current distributions on the Omega-shaped graphene-pattern metasurface at the non-resonance frequency and resonance frequency are displayed in Fig. 5. At the resonance frequency, the surface currents on the Omega-shaped graphene-pattern layer and the ground plane had the same direction. The strong plasmon resonances can effectively trap the incoming power, and the graphene losses provide an opportunity to dissipate this power.

The relationships among the absorption of TE and TM polarization modes, operating frequency, and incidence angle are plotted in Figs. 6a and 6b. In the figure, the absorber had a relatively stable absorption and absorption bandwidth in the incident angle



**Fig. 5** Surface current distributions: (a) TE polarization at  $f=0.4$  THz; (b) TE polarization at  $f=1.5$  THz; (c) TM polarization at  $f=0.4$  THz; (d) TM polarization at  $f=1.5$  THz

The arrow represents the direction of current and the color indicates the intensity of the electric field

range of  $0\text{--}60^\circ$ . For the TE polarization wave (Fig. 6a), the absorption peak and absorption bandwidth of the designed absorber were reduced slightly when the incident angle exceeded  $50^\circ$ , but the absorption remained above 80% in the 1.45–1.93 THz frequency range at an incident angle of  $60^\circ$ , and the absorption remained above 90% in the 1.62–1.84 THz frequency range. As the incident angle increased, the absorption in TM-polarized mode decreased rapidly (Fig. 6b). When the incident angle was  $60^\circ$ , the absorption of the designed absorber also remained above 80% in the 0.822–1.84 THz frequency range. The tangential component of TM-polarized mode in the electric field decreased with the increase of  $\theta$ , and the direction component of TE-polarized mode did not change. For both polarization modes, the absorption spectrum had a slight blue shift. Although there was a slight blue shift and a certain decrease in absorption, the absorption of the absorber was still above 80% with an incident angle range of  $0\text{--}60^\circ$ . In addition, the absorption spectrum of the designed absorber remained unchanged at different azimuth angles from  $0^\circ$  to  $90^\circ$  (Fig. 6c). Based on the above analysis, we conclude that the designed absorber demonstrates strong, stable terahertz absorption. The plasmon resonance property is the main reason for the good angular stability performance (Bouchon et al., 2012). Furthermore, the variation of the incident field

over the graphene metasurfaces caused by the sub-wavelength dimensions of the designed Omega-shaped graphene structure can be neglected even at large incident angles. In Table 1, the designed terahertz absorber has a relatively large incident angle range.

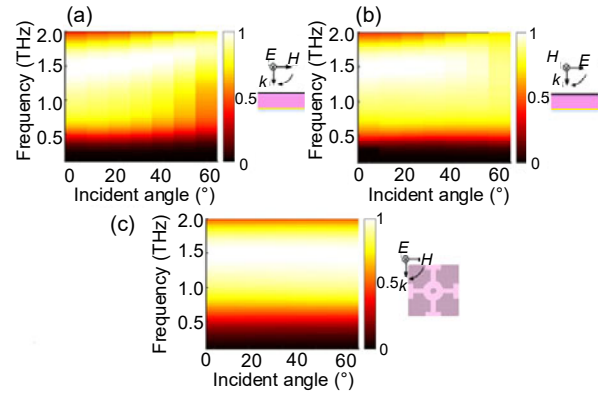


**Fig. 6** Absorption spectra with various incident angles for TE-polarized wave (a), TM-polarized wave (b), and the relationship between different azimuths and absorption spectra (c)

**Table 1** Performance comparison of our proposed absorber with some reported absorbers

| Reference           | Incident angle       | Pattern                        |
|---------------------|----------------------|--------------------------------|
| Song et al., 2020   | $0\text{--}45^\circ$ | Square-shaped vanadium dioxide |
| Daraei et al., 2020 | $0\text{--}40^\circ$ | Graphene ribbons               |
| This paper          | $0\text{--}60^\circ$ | Omega-shaped graphene          |

We also examined the absorption spectrum of the Omega-shaped graphene metasurface absorber when the relaxation time  $\tau$  of graphene changed from 0.2 to 0.4 ps with a pitch of 0.1 ps and other parameters remained unchanged (Fig. 7). When the relaxation time was  $\tau=0.2$  ps, the absorption reached 84% at  $f=0.62$  THz, and the absorption remained above 80% in the 1.28–1.86 THz frequency range. When the relaxation time was  $\tau=0.3$  ps, the absorption was 94% at 0.59 THz, and the absorption remained above 80% in the 1.46–1.85 THz frequency range. Finally, when  $\tau=0.4$  ps, the absorption was 98% at  $f=0.59$  THz, and was still above 80% in the 1.54–1.85 THz frequency range. Therefore, the designed Omega-shaped graphene metasurface absorber provides a new design for absorbers with narrowband or broadband absorption.

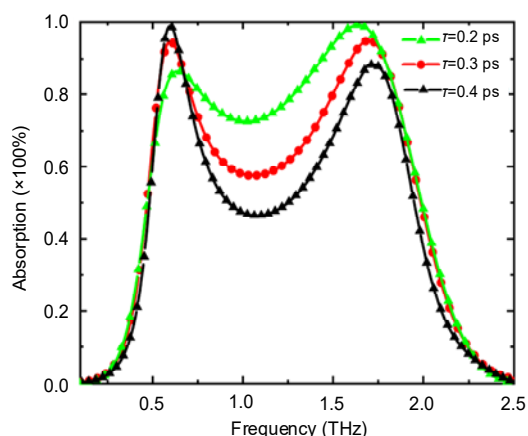


Fig. 7 Absorption spectra with different relaxation time  $\tau$

## 4 Conclusions

We have studied a terahertz wave absorber with an Omega-shaped graphene pattern. When the graphene chemical potential is 0.5 eV, the proposed absorber has perfect absorption (above 99.5%) in the 1.36–1.54 THz frequency range. The absorption is above 90% in the 1.05–1.69 THz frequency range. The absorption mechanism and polarization insensitivity have been explored based on the electric field distribution under TE and TM polarization modes. The proposed terahertz wave absorber achieves high absorption in the incident angle range of 0–60°. The characteristics of flexible tuning, wide incident angle range, and excellent absorption performance give it bright application prospects in dynamic modulators, sensors, switches, and other terahertz devices.

## Contributors

Jiu-sheng LI designed the research. Ri-hui XIONG processed the data and drafted the manuscript. Xiao-qing PENG helped organize the manuscript. Jiu-sheng LI revised and finalized the paper.

## Compliance with ethics guidelines

Ri-hui XIONG, Xiao-qing PENG, and Jiu-sheng LI declare that they have no conflict of interest.

## References

- Amin M, Farhat M, Bağcı H, 2013. An ultra-broadband multilayered graphene absorber. *Opt Expr*, 21(24):29938-29948. <https://doi.org/10.1364/oe.21.029938>
- Bouchon P, Koechlin C, Pardo F, et al., 2012. Wideband omnidirectional infrared absorber with a patchwork of

plasmonic nanoantennas. *Opt Lett*, 37(6):1038-1040.

<https://doi.org/10.1364/OL.37.001038>

Daraei OM, Goudarzi K, Bemani M, 2020. A tunable ultra-broadband terahertz absorber based on two layers of graphene ribbons. *Opt Laser Technol*, 122:105853.

<https://doi.org/10.1016/j.optlastec.2019.105853>

Esquiús-Morote M, Gómez-Díaz JS, Perruisseau-Carrier J, 2014. Sinusoidally modulated graphene leaky-wave antenna for electronic beamscanning at THz. *IEEE Trans Terahertz Sci Technol*, 4(1):116-122.

<https://doi.org/10.1109/TTHZ.2013.2294538>

He XY, Liu F, Lin FT, et al., 2019. Investigation of terahertz all-dielectric metamaterials. *Opt Expr*, 27(10):13831-13844. <https://doi.org/10.1364/OE.27.013831>

He XY, Lin FT, Liu F, et al., 2020a. Investigation of phonon scattering on the tunable mechanisms of terahertz graphene metamaterials. *Nanomaterials*, 10(1):39.

<https://doi.org/10.3390/nano10010039>

He XY, Lin FT, Liu F, et al., 2020b. Tunable strontium titanate terahertz all-dielectric metamaterials. *J Phys D*, 53(15):155105. <https://doi.org/10.1088/1361-6463/ab6ccc>

He YN, Zhang B, He T, et al., 2015. Optically-controlled metamaterial absorber based on hybrid structure. *Opt Commun*, 356:595-598.

<https://doi.org/10.1016/j.optcom.2015.08.070>

Hu FR, Zou TB, Quan BG, et al., 2014. Polarization-dependent terahertz metamaterial absorber with high absorption in two orthogonal directions. *Opt Commun*, 332:321-326.

<https://doi.org/10.1016/j.optcom.2014.06.017>

Jnawali G, Rao Y, Yan HG, et al., 2013. Observation of a transient decrease in terahertz conductivity of single-layer graphene induced by ultrafast optical excitation. *Nano Lett*, 13(2):524-530. <https://doi.org/10.1021/nl303988q>

Jo G, Choe M, Cho CY, et al., 2010. Large-scale patterned multi-layer graphene films as transparent conducting electrodes for GaN light-emitting diodes. *Nanotechnology*, 21(17):175201.

<https://doi.org/10.1088/0957-4484/21/17/175201>

Kim KS, Zhao Y, Jang H, et al., 2009. Large-scale pattern growth of graphene films for stretchable transparent electrodes. *Nature*, 457(7230):706-710.

<https://doi.org/10.1038/nature07719>

Liu TT, Jiang XY, Zhou CB, et al., 2019a. Black phosphorus-based anisotropic absorption structure in the mid-infrared. *Opt Expr*, 27(20):27618-27627.

<https://doi.org/10.1364/OE.27.027618>

Liu TT, Jiang XY, Wang HX, et al., 2019b. Tunable anisotropic absorption in monolayer black phosphorus using critical coupling. *Appl Phys Expr*, 13(1):012010.

<https://doi.org/10.7567/1882-0786/ab6270>

Liu Y, Zhong RB, Huang JB, et al., 2019. Independently tunable multi-band and ultra-wide-band absorbers based on multilayer metal-graphene metamaterials. *Opt Expr*, 27(5):7393-7404. <https://doi.org/10.1364/OE.27.007393>

Long YF, Chen X, Cai GX, et al., 2018. Electrically tunable broadband terahertz absorption with hybrid-patterned

- graphene metasurfaces. *Nanomaterials*, 8(8):562.  
<https://doi.org/10.3390/nano8080562>
- Othman MAK, Guclu C, Capolino F, 2013. Graphene-based tunable hyperbolic metamaterials and enhanced near-field absorption. *Opt Expr*, 21(6):7614-7632.  
<https://doi.org/10.1364/OE.21.007614>
- Shi CYY, He XY, Peng J, et al., 2019. Tunable terahertz hybrid graphene-metal patterns metamaterials. *Opt Laser Technol*, 114:28-34.  
<https://doi.org/10.1016/j.optlastec.2019.01.024>
- Song ZY, Jiang MW, Deng YD, et al., 2020. Wide-angle absorber with tunable intensity and bandwidth realized by a terahertz phase change material. *Opt Commun*, 464:125494. <https://doi.org/10.1016/j.optcom.2020.125494>
- Su ZX, Yin JB, Zhao XP, 2015. Terahertz dual-band metamaterial absorber based on graphene/MgF<sub>2</sub> multilayer structures. *Opt Expr*, 23(2):1679-1690.  
<https://doi.org/10.1364/OE.23.001679>
- Xiao SY, Wang T, Liu YB, et al., 2016. Tunable light trapping and absorption enhancement with graphene ring arrays. *Phys Chem Chem Phys*, 18(38):26661-26669.  
<https://doi.org/10.1039/c6cp03731c>
- Xiao SY, Liu TT, Cheng L, et al., 2019. Tunable anisotropic absorption in hyperbolic metamaterials based on black phosphorous/dielectric multilayer structures. *J Lightw Technol*, 37(13):3290-3297.  
<https://doi.org/10.1109/JLT.2019.2914183>
- Zhang JF, Liu WB, Zhu ZH, et al., 2016. Towards nano-optical tweezers with graphene plasmons: numerical investigation of trapping 10-nm particles with mid-infrared light. *Sci Rep*, 6:38086.  
<https://doi.org/10.1038/srep38086>
- Zhang Y, Feng YJ, Zhu B, et al., 2014. Graphene based tunable metamaterial absorber and polarization modulation in terahertz frequency. *Opt Expr*, 22(19):22743.  
<https://doi.org/10.1364/OE.22.022743>
- Zhang YB, Tan YW, Stormer HL, et al., 2005. Experimental observation of the quantum Hall effect and Berry's phase in graphene. *Nature*, 438(7065):201-204.  
<https://doi.org/10.1038/nature04235>
- Zhou RY, Wang C, Xu WD, et al., 2019. Biological applications of terahertz technology based on nanomaterials and nanostructures. *Nanoscale*, 11(8):3445-3457.  
<https://doi.org/10.1039/C8NR08676A>